tributions.[4,5] At 0.93 Bev, the agreement of the calculations with the data is reasonably good. The observed π^- spectrum has a broad momentum distribution, while the π^+ spectrum has a maximum at high momenta (0.35–0.40 Bev/c), as is expected from the present model. However, at 1.37 Bev, the predicted π^+ spectrum is in disagreement with the data, and there is an indication that the fraction of the recoil pions which are π^+ is smaller than would be obtained from the isobar model.

It should be mentioned that the particular isobar theory proposed here can only be applied directly to single pion production in pion-nucleon collisions. At energies above $\sim$1.5 Bev, where double production becomes important, one would have to consider modifications of the present treatment of the isobar model. One such possibility is that two or more recoil pions are coupled to the $T=J=\frac{3}{2}$ isobar at these higher energies. It is also possible that a different isobar having $T=\frac{1}{2}$, $\frac{3}{2}$, $\frac{5}{2}$, or $\frac{7}{2}$ with the same or different J values is involved in cases where double pion production takes place. Even at the higher energies ($\gtrsim$1.5 Bev), where double production plays an important role, the single pion production may still proceed primarily via the $T=J=\frac{3}{2}$ state and would then be described by the present treatment. However, a different single production isobaric level could become important.

The predictions of the isobar model are markedly different from the results of the statistical theory. Therefore, when better experimental data become available, it should be relatively simple to discriminate between the two models. At 0.93 Bev, although the statistics are limited and the momentum intervals of the data are rather wide, the over-all pattern of the experimental results is in much better agreement with the isobar model than with the statistical theory. At 1.37–1.5 Bev, some of the predictions, notably the combined pion spectra, seem to agree reasonably well with the data. However, the calculated separate π^+ spectrum seems to be in disagreement, but the statistics are quite limited for this spectrum. The very limited statistics and other errors in the available data at 1.37–1.5 Bev make it difficult to draw any definite conclusions about the general validity of the isobar model in this energy range.

PHYSICAL REVIEW VOLUME 109, NUMBER 5 MARCH 1, 1958

Interactions of 38- and 61-Mev Positive Pions in Deuterium*†

A. M. Sachs, H. Winick,‡§ and B. A. Wooten
Nevis Cyclotron Laboratory, Columbia University, Irvington-on-Hudson, New York

(Received August 26, 1957)

Measurements have been made of the reactions (1) $\pi^+ + d \rightarrow \pi^+ + d$, (2) $\pi^+ + d \rightarrow \pi^+ + n + p$, and (3) $\pi^+ + d \rightarrow p + p$ at incident pion lab energies of 38 and 61 Mev using a liquid deuterium target and scintillation counters. A separation of the three processes is obtained by determining the mass and energy of reaction products using a pulse-height analysis technique on the signals from the scintillation counters. Results from process (3) are compared with other processes involving two nucleons and a meson and results from processes (1) and (2) are compared with impulse approximation calculations.

I. INTRODUCTION

WHEN positive pions are incident on deuterons the following five reactions may proceed:

$$\pi^+ + d \rightarrow \pi^+ + d \quad \text{(elastic scattering)}, \quad (1)$$
$$\rightarrow \pi^+ + n + p \quad \text{(inelastic scattering)}, \quad (2)$$
$$\rightarrow p + p \quad \text{(nonradiative absorption)}, \quad (3)$$
$$\rightarrow \pi^0 + p + p \quad \text{(charge exchange scattering)}, \quad (4)$$
$$\rightarrow \gamma + p + p \quad \text{(radiative absorption)}. \quad (5)$$

Much of the previous work on the interactions of pions in deuterium has been concerned with the measurement of the total cross section for all five processes.[1–3] The nonradiative absorption process was the first to be individually measured,[4] because of its significance in determining the spin of the pion. More recently attempts have been made to measure the cross sections for individual processes in counter experiments at 119 Mev,[5,6] 94 and 76 Mev,[7] and 45 Mev.[8] The most complete work has been done at 85 Mev,[9] where cross sections for each

* This research is supported by the Office of Naval Research and the U. S. Atomic Energy Commission.

† This research was initiated in conjunction with Professor D. Bodansky, University of Washington, who designed much of the equipment and participated in the early stages of the experiment while he was at Columbia.

‡ Submitted by H. Winick in partial fulfillment of the requirements for the degree of Doctor of Philosophy in the Faculty of Pure Science, Columbia University.

§ Present address: University of Rochester, Rochester, New York.

[1] Isaacs, Sachs, and Steinberger, Phys. Rev. **85**, 803 (1952).
[2] Anderson, Fermi, Nagle, and Yodh, Phys. Rev. **86**, 4136 (1952).
[3] Ashkin, Blaser, Feiner, Gorman, and Stern, Phys. Rev. **96**, 1104 (1954).
[4] Durbin, Loar, and Steinberger, Phys. Rev. **84**, 581 (1951).
[5] C. Cohen, Phys. Rev. **105**, 1582 (1957).
[6] D. Nagle, Phys. Rev. **97**, 480 (1955).
[7] H. Stadler, Phys. Rev. **96**, 496 (1954).
[8] D. Bodansky and A. Sachs, Phys. Rev. **98**, 240(A) (1955).
[9] K. C. Rogers and L. M. Lederman, Phys. Rev. **105**, 247 (1957).

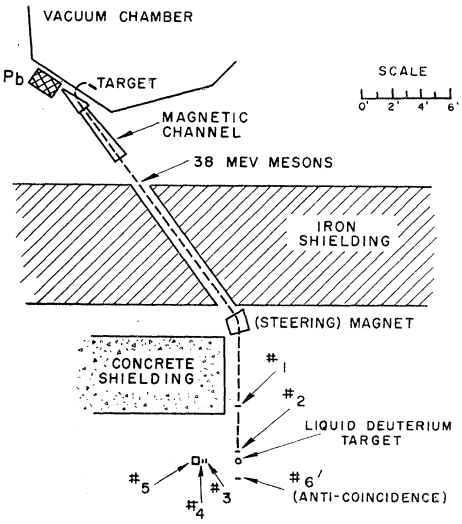

FIG. 1. Experimental arrangement for the 38-Mev experiment. For the 61-Mev experiment, the arrangement is identical except for the absence of the magnetic channel.

of the five processes were measured in a diffusion cloud chamber.

Theoretical predictions of the individual cross sections for processes (1), (2), and (4) are available from impulse approximation calculations.[10,11] These calculations treat the $\pi-d$ interaction phenomenologically in terms of the $\pi-n$ and $\pi-p$ interactions, the characteristics of which are inserted into the theory in the form of the experimentally determined phase shifts. Also, semiempirical analysis of all experiments involving emission and absorption of pions by a system of two nucleons has been made[12,13] assuming charge independence and s- and p-wave interactions only. Cross sections for process (3) may be compared with the results of this treatment.

This experiment is an attempt to measure the individual cross sections for processes (1), (2), and (3). These reactions are detected by observing the scattered pion in reactions (1) and (2), and one of the protons in reaction (3). In order to separate these processes, the mass and energy of reaction products are determined by analyzing the pulse heights of signals from three scintillation counters.

II. EXPERIMENTAL METHOD

A. General

The experimental arrangement used in the 38-Mev experiment is shown in Fig. 1. A beam of 42 ± 4 Mev pions was extracted directly from the cyclotron by using an iron magnetic channel installed just outside the cyclotron vacuum chamber. This channel, designed by Koppel *et al.*,[14] decreased the fringing field of the cyclotron magnet in the region between the magnet coils, permitting pions with energy as low as 30 Mev to escape. At 63 Mev, the channel is not necessary, and the experimental arrangement is identical to that of Fig. 1 with the channel removed.

After emerging from a hole in the 8-ft thick iron shield, the mesons are analyzed by a double-focusing magnet. The beam, defined by counters 1 and 2, is then incident on a liquid deuterium target. Reaction products emerging from the target are analyzed in a three-counter telescope (counters 3, 4, 5). Counter 4, $22\frac{3}{4}$ in. from the center of the target, defines the effective solid angle. An anticoincidence counter (6′) aids in reducing accidental background. Measurements are made at 45°, 60°, 90°, 113°, 135°, and 150° to the incident beam using the following procedure. The system is first calibrated by placing the detection telescope in line with the incident beam (0°) position. The detection telescope is then moved to one of the above angles, and measurements are made alternately with target cup full of liquid deuterium and empty. Before measurements are made at a different angle the detection telescope is returned to 0° to check on the stability of the equipment.

B. Target

The scattering chamber consists of a 3.1-in. diameter and 0.004 in. thick stainless steel cylindrical cup filled with liquid deuterium, or liquid hydrogen, in a metal Dewar which has been previously described.[15] The deuterium is contained in a closed system and is liquefied by being brought into thermal contact with liquid hydrogen. The target cup may be filled from a liquid deuterium reservoir and may be emptied by closing its exhaust line and applying heat via a small resistance element located at the bottom of the cup.

C. Counters

The pertinent facts about the counters are contained in Table I. The plastic scintillating material, styrene with terphenyl and tetraphenylbutadiene, was polymerized at this laboratory. Considerable care was taken to make counters 3, 4, and 5, as uniform as possible, since they are used for pulse-height analysis.

TABLE I. Description of counters.

Counter	Size of plastic scintillator	Phototubes
1	3 in.$\times 2\frac{1}{2}$ in.$\times\frac{1}{8}$ in.	2-1P21's
2	$2\frac{3}{8}$ in.$\times 2\frac{1}{4}$ in.$\times\frac{1}{8}$ in.	2-1P21's
3	3 in.$\times$6 in.$\times\frac{1}{4}$ in.	2-5819's
4	3 in.$\times$6 in.$\times\frac{1}{4}$ in.	2-5819's
5	$5\frac{1}{2}$ in.$\times$8 in.$\times$6 in.	6-5819's
6′	$5\frac{3}{4}$ in. diam$\times\frac{1}{2}$ in. thick	1-5819

[10] Fernbach, Green, and Watson, Phys. Rev. **84**, 1084 (1951).
[11] R. Rockmore, Phys. Rev. **105**, 256 (1957).
[12] M. Gell-Mann and K. Watson, *Annual Review of Nuclear Science* (Annual Reviews, Inc., Stanford, 1954), Vol. 4.
[13] A. Rosenfeld, Phys. Rev. **96**, 139 (1954).
[14] Koppel, Bingham, and Booth, Rev. Sci. Instr. **28**, 645 (1957).
[15] Bodansky, Sachs, and Steinberger, Phys. Rev. **93**, 1367 (1954).

Counter 5 consists of a large block of plastic scintillator painted on five faces with a high reflectance white paint for diffuse reflection. The 6-in. depth of the plastic scintillator of counter 5 is sufficient to stop the most energetic pion or proton available in this experiment. Each of the six photomultipliers which view counter 5 from the rear has an individual potentiometer in series with its high voltage. These controls are used to optimize the uniformity of response by adjusting the relative sensitivities of the photomultipliers to compensate for variation in light collecting efficiency from different parts of the plastic scintillator.

A test of the uniformity of counters 4 and 5 indicated that for counter 4 (and presumably also for 3, which is identical to 4) the maximum variation of pulse height over 4 in. of its 6-in. dimension is $\pm 1.5\%$ while for counter 5, the maximum variation of the pulse height over a 4 in.$\times$6 in. rectangle is $\pm 3\%$.

D. Electronics

Figure 2 shows a block diagram of the electronics. Positive signals taken in parallel from the photomultipliers of counters 1 and 2 and negative signals from the lower phototubes of counters 3 and 4 are amplified in Hewlett Packard wide-band amplifiers. Double coincidences, with a resolving time of approximately 10^{-8} sec, are then made between counters 1 and 2, 3 and 4, and 2 and 4 in a diode bridge coincidence circuit. These double coincidence signals are then fed into an amplifier, discriminator, and EFP-60 pulse shaper and then into a second coincidence circuit where a coincidence of 10^{-7} sec resolving time is made among 12–24–34. This coincidence defines an event, the 24 coincidence being included in order to lower the effective resolving time between incident and detecting telescopes to 10^{-8} sec, thereby minimizing accidentals.

The pulse-height system is also indicated on the block diagram. The signals from the photomultipliers of counters 3, 4, 5, and 6′ are delayed by different amounts of cable and fed into a mixing circuit. The output of the mixing circuit is then fed into a series of Hewlett Packard wide-band amplifiers which were modified for operation from a regulated external power supply. The output of the last of these amplifiers is fed directly to the vertical plates of the cathode ray tube of an oscilloscope designed to photograph single traces. The output of the 12–24–34 coincidence circuit is used to trigger the sweep circuit of the oscilloscope which then displays the signals from counters 3, 4, 5, and 6′ on a trace at a sweep speed of 0.1 μsec/cm. The trace is photographed on 35 mm film by a General Radio Oscillograph Recorder which has been adapted by replacing its motor drive with an automatic stepping switch to advance the film. A Lucite screen with 65 horizontal parallel lines, each 0.001 in. thick, engraved on it, is placed in contact with the face of the cathode ray tube. After each trigger, before the film is advanced,

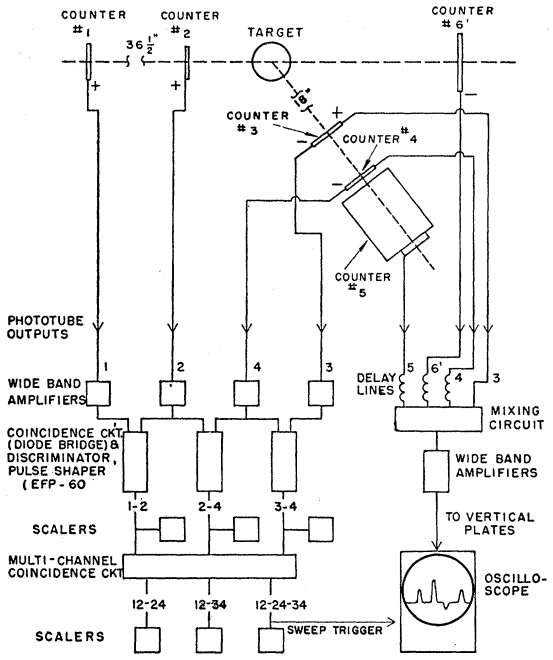

FIG. 2. Block diagram of electronics.

neon bulbs in the screen are flashed, providing a convenient scale for measuring pulse heights on each frame. 3000 traces are photographed on each 100-foot roll of film. 100 000 oscilloscope pictures were taken in this experiment, one-half of which were for calibration and one-half data.

E. Pulse-Height Analysis

In addition to the incident flux, as measured by the 1–2 scaler, the essential data of the experiment consist of the oscilloscope photographs. The film is projected on a screen and read by a scanner using a dictaphone to record the heights of the signals from counters 3, 4, and 5. The presence or absence of a properly timed negative signal from counter 6′ is also noted. A signal from counter 6′ indicates that the particle that went through counters 1 and 2 did not interact in the target, and hence the coincidence is accidental. The detection of these accidentals in this manner is not 100% efficient since, in order to minimize counts in 6′ due to recoil protons and deuterons, it was set 15 in. behind the center of the target cup and thus intercepts only 85% of the beam going through 1 and 2. A record of the number of these accidental coincidences in each run indicates that there is no systematic difference in the efficiency of counter 6′ during deuterium and background runs.

Events that do not have a signal from counter 6′ (i.e., real events) may also be rejected if the pulse heights of signals from counter 4 or 5 cannot be reliably read due to distortion of these pulses caused by the accidental overlap of other positive or negative signals. It is important that only random overlaps be rejected, so that

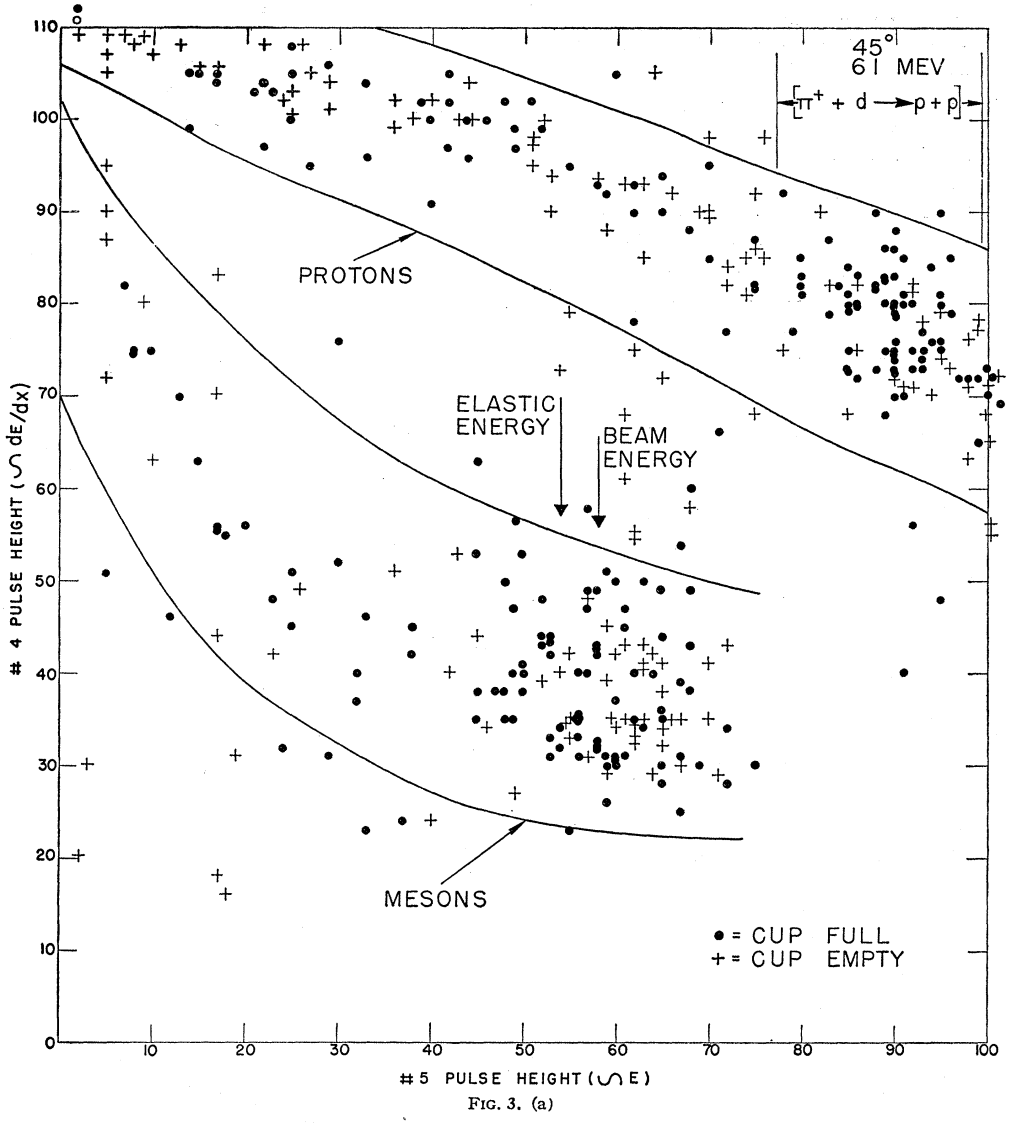

FIG. 3. (a)

no systematic error is introduced. An example of a non-random overlap would be the small positive signals that may appear on the trailing edge of the signals of counter 5. These are due to muons which come from the pion decay in counter 5. A set of criteria is established so that only random overlaps are cause for rejection of otherwise good data. Approximately 8% of the real events were rejected on this basis, and the calculated cross sections were adjusted accordingly.

Events that have not been rejected are transcribed from the dictaphone recordings to graphs where the pulse height in counter 4 is plotted *versus* the pulse height in counter 5. Counters 3 and 4 are thin and their pulse heights are therefore an approximate measure of the particle's specific ionization, dE/dx. Counter 5 is thick enough to stop the most energetic particles that emerge from the target in this experiment, and hence the pulse height of the signal from this counter is proportional to the total kinetic energy E of the particle. Therefore, if the pulse height from counter 3 or 4, (dE/dx), is plotted *versus* the pulse height from counter 5, (E), the result is a family of curves, approximately hyperbolic in shape, each characterized by a different value of particle mass m. For this experiment, the result, in principle, is a set of two such curves separated from each other by an amount determined by the relative masses of the pion and proton. Thus a plot of the pulse height in counter 4 *versus* the pulse height in counter 5 performs the two required functions of separating protons from pions and providing an energy determination for the pions.

In Fig. 3 are presented typical graphs of pulse height in counter 4 *versus* pulse height in counter 5 due to events recorded at 45°, 90°, and 135° to the incident 63-Mev beam. The vertical spread of the proton and meson bands is caused almost entirely by statistical

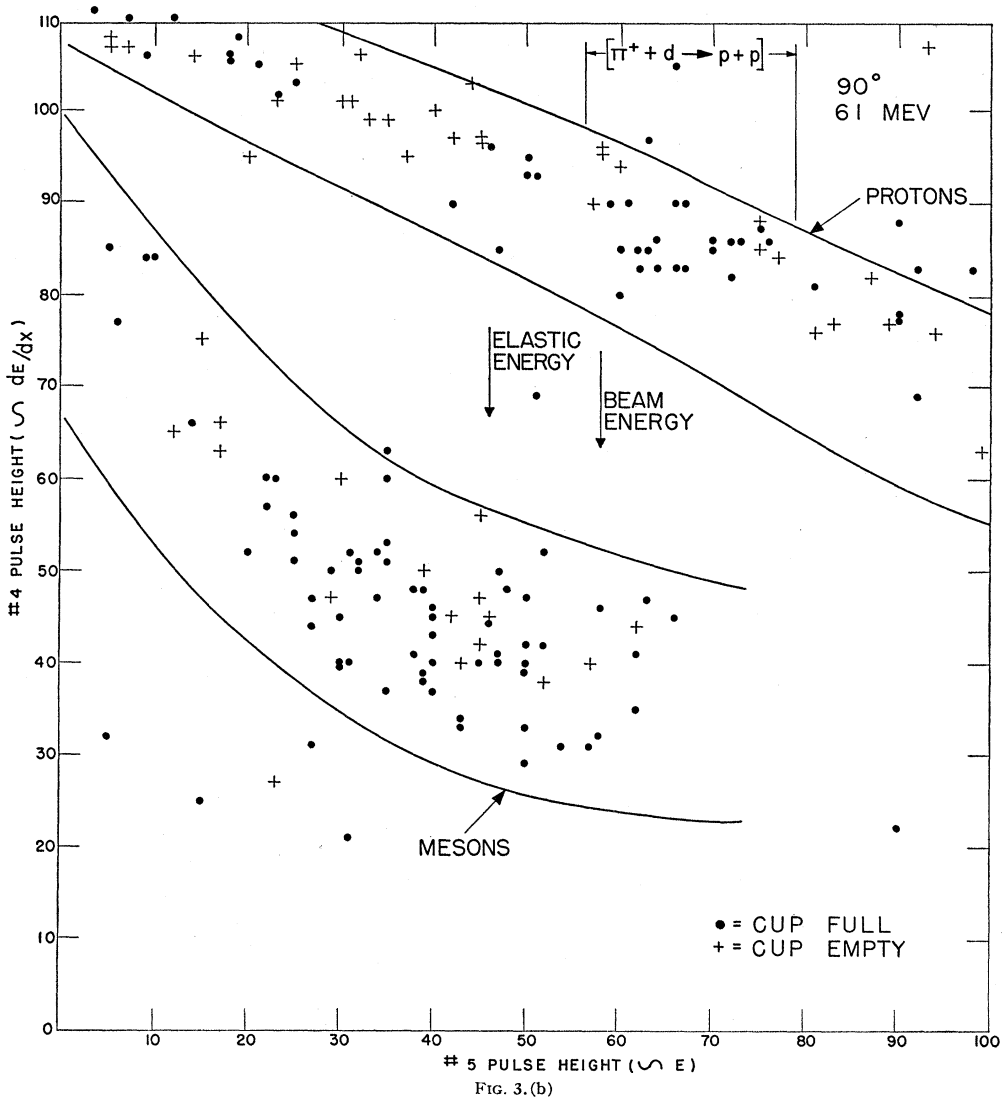

FIG. 3.(b)

fluctuations in energy loss in counter 4. Each of these graphs represents the data recorded in one hour at one angle for 3.6×10^6 incident pions, half of which are with liquid deuterium in the cup and the other half with the cup empty.

In the indicated regions of the proton bands, the net deuterium effect is due to protons from the nonradiative absorption process. The median energy of this group is observed to decrease as the angle increases according to the kinematics of the process. There is no statistically significant deuterium effect in the proton band on either side of this group.

The variation of the background with angle may also be seen from these graphs. For both mesons and protons the background is greatest at 45° and least at 90°. The ratio of the net deuterium effect (cup full minus cup empty), to the background (cup empty) at 63 Mev is presented in Table II for pions and protons at each angle. For the protons, the ratio is presented for the entire proton band and also for the section of this band which is relevant to the nonradiative absorption process. The ratio of net deuterium effect to background at 42 Mev is not shown but is lower by a factor of about 2 in all cases due primarily to the smaller deuterium cross sections.

Many of the points that remain in the region between meson and proton bands after elimination of the

TABLE II. Ratio of net deuterium effect to background (61 Mev).

	45°	60°	90°	113°	135°	150°
Mesons	0.56	1.44	3.09	2.73	2.15	1.31
Protons in entire band	0.65	0.48	0.76	1.18	0.83	0.66
Protons in relevant region	2.94	2.21	2.33	3.27	2.50	2.00

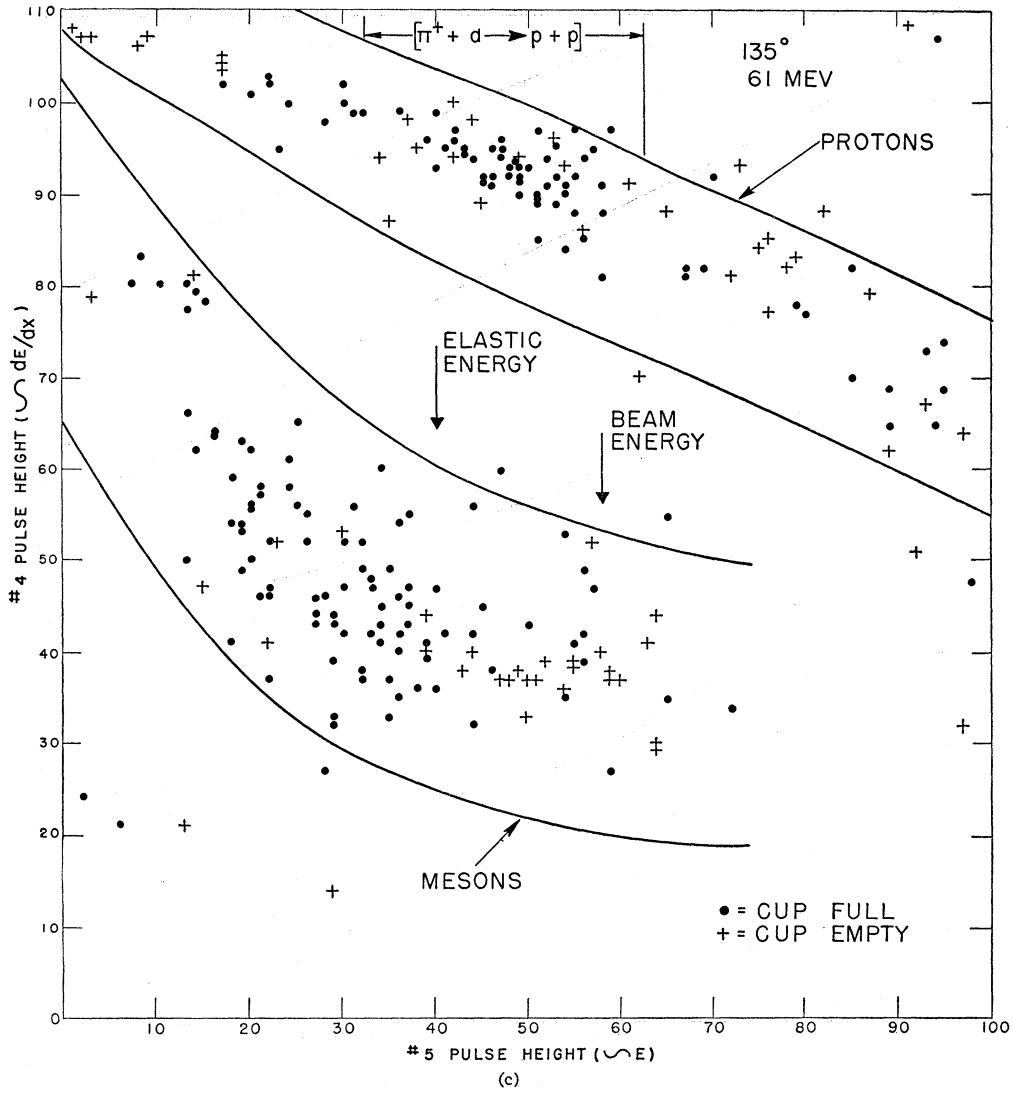

FIG. 3. Typical graphs of data at 61 Mev (bands drawn are illustrative only).

accidentals detected by counter 6′ are due to large fluctuations of energy loss in counter 4. In these cases, an examination of the pulse height from the other thin counter, (3), helps to reveal whether the particle was a proton or pion.

From graphs, such as those presented in Fig. 3, energy distributions of background protons and pions may be obtained at each angle, and analysis of these distributions yields information on the origin of the background and its possible modification due to the presence of the deuterium.

III. CALIBRATION MEASUREMENTS

A. Incident Beam Energy and Composition

The composition, mean energy, and spread in energy of both the 42-Mev and 63-Mev incident beams were determined from the integral range curves shown in Fig. 4. The fraction of muons in the beam may be estimated from the height of the plateau between the sharp drops in the range curve. A more accurate value for the μ percentage is then calculated as that which makes the resulting momentum distributions of incident pions and muons most nearly the same.

The total beam contaminations (muons plus positrons) obtained in this manner are 12.3% for the 42-Mev beam and 10.5% for the 63-Mev beam. The 42-Mev beam had a 2% positron contamination and the 63-Mev beam had less than 1% positrons. After subtracting the mean energy loss in counters 1 and 2 and in the target, values of 37.6 ± 4 Mev and 60.7 ± 3 Mev are obtained for the mean energies of pions before interaction in the deuterium.

B. Scattered Beam Energy

An energy calibration for scattered mesons is obtained by placing the detection telescope in line with the incident beam. Photographs are taken of the pulse heights produced by this beam and by beams of lower energy obtained by slowing down the incident beam in various thicknesses of carbon absorber. A plot of pulse height in counter 4 *versus* pulse height in counter 5 is then made on the same graph for each of these runs. An example of such a graph is given in Fig. 5. Although in the runs with no absorber it is not possible to separate the π's and the μ's, upon inserting absorber the π's are preferentially degraded in energy leaving a separation between π's and μ's. The μ contamination measured in this manner is in agreement with the value obtained from the range curve analysis. For the cases in which the meson had insufficient range to reach counter 5, a plot of pulse height in counter 3 *versus* pulse height in counter 4 is used to extend the usable range of the system to lower energy.

After correcting for the beam contamination, the median of each of the groups of points in Fig. 5 yields the mean pulse height produced in counter 5 by pions of known energy. These medians are then used to obtain a calibration curve of pion pulse height in counter 5 *versus* mean energy at the center of the target (see Fig. 6). In addition to their use in obtaining these energy calibrations, graphs such as Fig. 5 also serve to delineate the entire meson band for the angular runs.

A proton energy calibration is not essential since only nonradiative absorption is being measured. The following check was made however to make certain that the pronounced peaks in the proton band came from the nonradiative absorption process. With the detection telescope at 135° to the incident 42-Mev beam, counter 6 was moved from its 0° position to −35° to the incident beam in order to count the other emitted proton. Ninety-five percent of the net deuterium effect in the region of the pronounced peak was observed to be due to events which also had a signal from counter 6, the 5% loss being consistent with the number of related protons calculated to fall outside the solid angle subtended by 6.

The vertical spread of the meson and proton bands on the graphs is due almost entirely to the statistical fluctuation in energy loss in the thin counters. This problem has been treated theoretically by Symon.[16] The results of a calculation based on his work for the predicted spread in pulse height from a $\frac{1}{4}$-in. stilbene crystal is indicated in Fig. 5. The curved lines on that figure form a band which, according to Symon's results, should contain 80% of the pions. The band does contain $(72\pm7\%)$ of the pions indicating that almost all of the spread may be accounted for in this way.

In order for a pion to escape the deuterium cup, pass through counter 3, and penetrate far enough into counter 4 to be detected (thus triggering the oscilloscope), it must have a mean energy of at least 16 Mev after scattering. Therefore, pions which are scattered with mean energy less than 16 Mev are not recorded in this experiment. All of the elastically scattered mesons have energies considerably above 16 Mev so that this threshold for detection does not affect measurements of the elastic cross section. The lowest energy proton from the nonradiative absorption process is the 66-Mev proton that emerges at 150° to the incident 42-Mev pion beam, and this is higher than the 37-Mev detection threshold for protons.

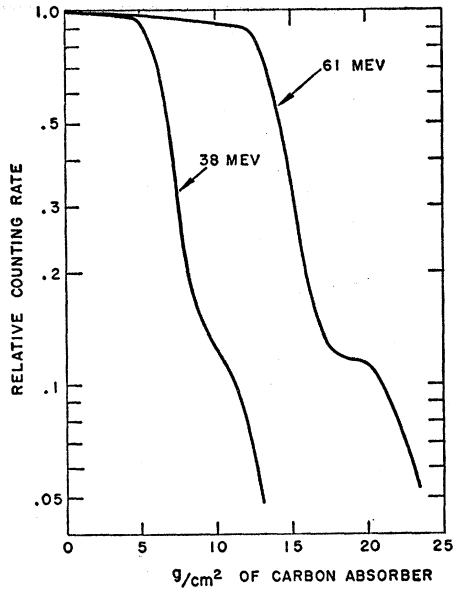

FIG. 4. Range curves.

C. Stability Checks

Because the pulse height from counter 5 is used directly to determine the energy of the scattered pion, and the pulse heights from counters 3 and 4 are used to separate pions from protons, it is essential to maintain stability in the pulse-height system. Meters that monitor the operation of each of the electronic elements of the pulse-height system are read and recorded periodically. In addition, a check is made on the gain of the system before and after each angular run. This is done by placing the detection telescope in line with the incident beam, reducing the cyclotron intensity, and photographing the pulse heights produced by this beam, as is done to obtain the energy calibration. A polaroid camera is also used to take a multitrace photograph of the oscilloscope. The distribution of pulse heights in each of the counters is recorded on this photograph as a slight smearing. (See Fig. 7.) The median pulse height in the counters can be reliably read from the photograph, and if a drift has occurred, it may be corrected before the next angular run is started.

[16] K. Symon, thesis, Harvard University, 1948 (unpublished). Parts of this work appear in B. Rossi, *High-Energy Particles* (Prentice Hall, Inc., New York, 1952).

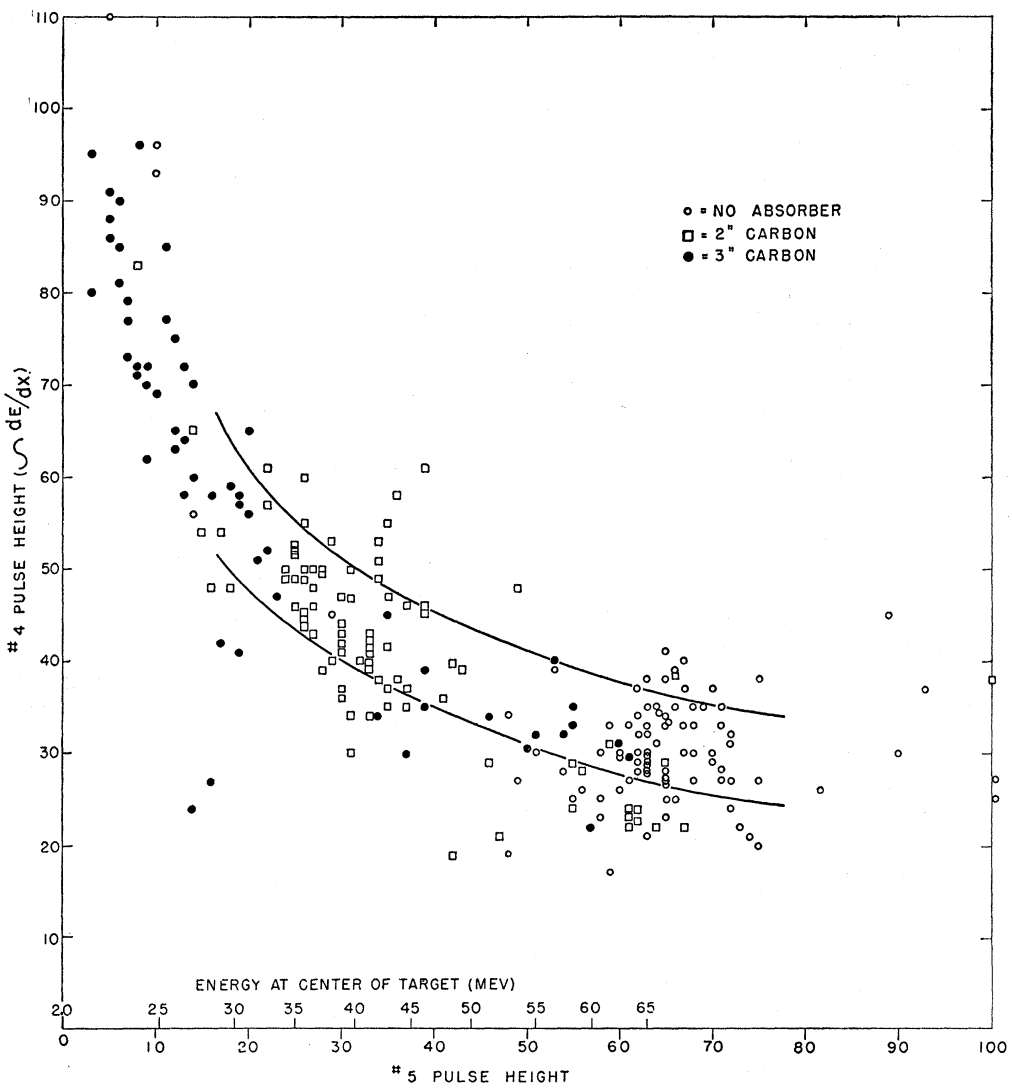

FIG. 5. 0° graph (61 Mev). The solid lines form a band which should contain 80% of the pion points according to a calculation based on Symon's theory.

D. Angular Resolution

A measure of the angular resolution of the detection telescope is obtained by recording the relative counting rates as the telescope is rotated through the forward angles. For both 42- and 63-Mev beams, the counting rate drops by a factor of 2 when the telescope is rotated in either direction to 5° from the incident beam.

IV. EXPERIMENTAL RESULTS

The uncorrected experimental results are presented in Figs. 8 through 11, which give energy distributions of the net deuterium effect for emergent mesons and protons for both incident beam energies. To obtain the net deuterium effect in a given energy interval, a direct subtraction is made of background points in this interval from points in the same energy interval obtained with the cup full. Thus these distributions contain no corrections for possible effects of the deuterium on the background.

The first four intervals of the meson histograms have been averaged, because the energy calibration is uncertain in this region. The vertical scale on each of the histograms presented in Figs. 8 through 11 indicates the net number of counts due to deuterium in each energy interval per 4.1×10^6 particles passing through the incident beam telescope.

V. CALCULATION OF CROSS SECTIONS

A. Experimental Parameters

The experimental results are used to obtain uncorrected laboratory differential cross sections by using the

relation

$$(d\sigma/d\Omega)_{\text{Lab}}=N/(\Omega\alpha\epsilon t\rho). \quad (6)$$

N, the net number of counts from deuterium (cup full minus cup empty) per particle passing through the incident beam telescope, is obtained directly from the experimental data. Ω, the solid angle defined by counter 4, is 0.0344 steradian. α, the fraction of the incident beam which is pions, is 0.877 for the 42-Mev beam and 0.895 for the 63-Mev beam. The efficiency for detecting emerging particles, ϵ, is computed from a measurement of the efficiency for detecting particles which are known to pass through the telescope, and an estimate of the loss of counts from the meson and proton bands because of nuclear interactions in the counters. For mesons $\epsilon=0.94$ and for protons $\epsilon=0.96$.

The mean thickness of the deuterium, t, is 6.43 cm and was obtained by folding the horizontal beam profile into the 3.1 in.-diameter circular target cup. The profile is measured at two distances behind the target cup by scanning with a $\frac{1}{8}$-in. crystal, and an extrapolation is used to obtain the beam profile at the target cup. The effective density of deuterium, ρ, is taken as 5.00×10^{22} atoms per cc for the meson scattering, and 4.89×10^{22} atoms per cc for the nonradiative absorption. The first of these is the density of the liquid[17] minus the density of gas at 20.5°K. The temperature is estimated from the temperature of liquid hydrogen (20.4°K) at atmospheric pressure, and the boiling point (20.6°K) of deuterium at the measured equilibrium pressure of the deuterium gas reservoir. An analysis of a sample of the deuterium used in this experiment revealed that it contained 97.7% deuterium, with hydrogen constituting the major contamination. Since the scattering of positive pions from hydrogen is similar to that from deuterium, no correction was made for the small hydrogen contamination in computing the meson scattering cross sections. However, the value of ρ given for nonradiative absorption includes this correction.

B. Corrections from π-μ Decay and Multiple Scattering

At the mean velocity after scattering, 10% of the pions will decay before reaching counter 4. Some of the μ's from pion decay will trigger the detection system, giving pulse heights similar to those from pions because of the small mass difference. Some of the pions however, which originally would have been detected will decay into muons which will miss the detection telescope, resulting in a loss of counts. Other pions, whose original scattered direction was not in the angular interval defined by the detection system, will decay into muons which will trigger the system resulting in a gain in counts. A similar loss and gain of counts results from multiple scattering of pions and protons in the deuterium and in counter 3. The largest multiple scattering effect is for pions passing through counter 3, where the mean multiple-scattering angle varies from 2° at 50 Mev to 6° at 16 Mev. In the 6° case, 7% of the pions that would have passed through counter 4 are lost due to multiple scattering in counter 3, with correspondingly smaller losses for the smaller multiple scattering angles.

For both the $\pi-\mu$ decay and the multiple scattering' calculations indicate that the loss in counts due to decays and multiple scatterings out of the detection system approximately equals the gain due to decays and multiple scatterings into the detection system. Therefore no correction for these effects was made on the cross sections. Since only 10% or less of the reaction products are involved in these effects, if the calculation is in error by as much as 20%, at most a 2% error will be introduced into the final cross section.

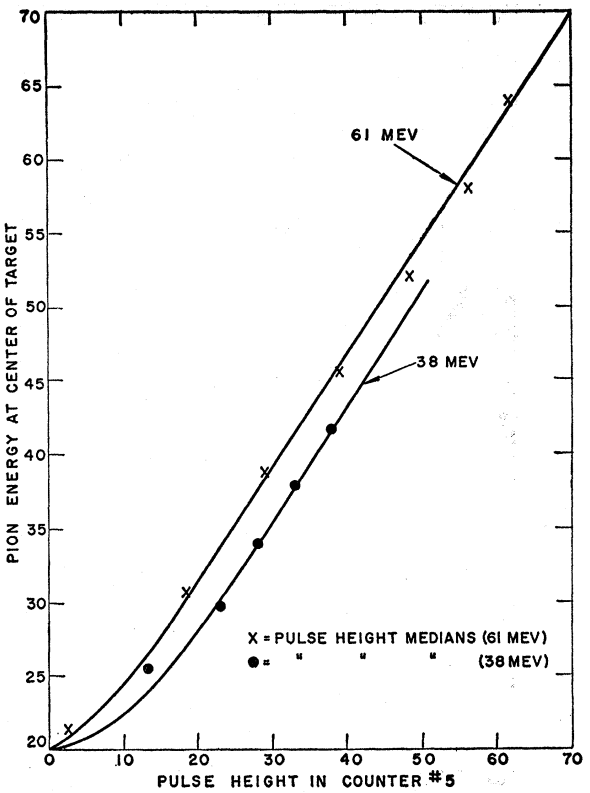

FIG. 6. Energy calibration curves. These curves are used to transform the observed pulse height in counter 5 to energy at the center of the target.

C. Effect of Deuterium on Background

To compute the cross section for scattering with final pion energy greater than 16 Mev, it is necessary to estimate how much of the background is lost because of energy loss by ionization in the deuterium when the cup is full. The only part of the background which could possibly be lost in this manner is the low-energy end from 16 Mev to 24 Mev, since the higher energy background will have enough energy left to trigger the

[17] Wooley, Scott, and Brickwedde, J. Research Natl. Bur. Standards 41, 379 (1948).

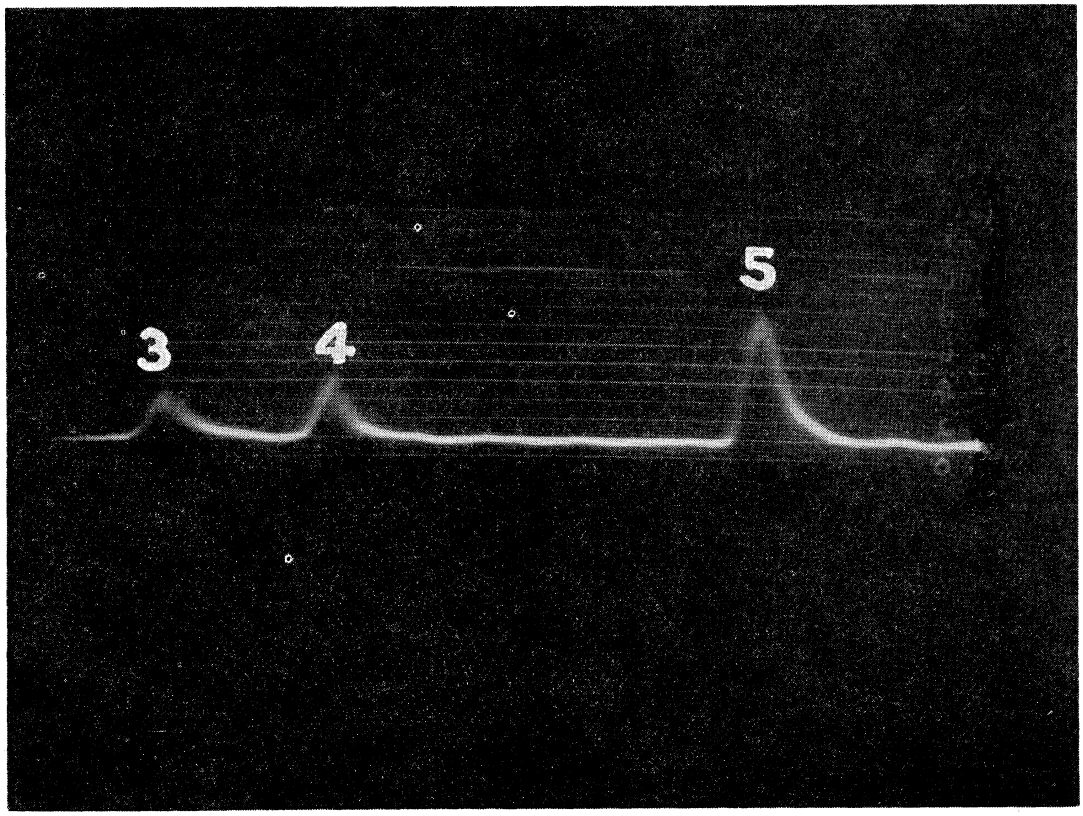

FIG. 7. Typical polaroid photograph of oscilloscope traces at 0 deg.

detection system even after passing through the full deuterium thickness.

Energy distributions of the pion background indicate that the 16–24 Mev interval contains only a small part of the total background. Consideration of the origin of the background indicates that no more than one third of the background is likely to pass through the deuterium. At 61 Mev, for all angles except 45 degrees, this upper limit leads to a correction which would increase the scattering cross sections by less than 1%. Therefore, no corrections were made for these cross sections. For 45 degree scattering at 61 Mev and for all scattering angles at 38 Mev, a correction was made based on the estimate that 20±20% of the background passes through the deuterium. The resultant increases at 38 Mev are 2.7±2.7% at 60°, 90°, 113°, and 135° and 4±4% at 150°. At 45° the large ratio of background to deuterium counts makes this correction larger, increasing the cross section by 3.6±3.6% at 61 Mev and 33±33% at 38 Mev. The errors due to the lack of precise knowledge of these corrections were compounded with the statistical errors for the scattering cross sections. The cross sections for scattering with final pion energy greater than 16 Mev are presented in Table III. For the nonradiative absorption process no corrections are necessary for the effect of deuterium on the background, since the small number of background protons are uniformly distributed over the entire range of energy detected. The cross section results for the nonradiative absorption process are presented in Table IV.

D. Elastic Scattering Cross Sections

Theoretically, there is a gap of 2.2 Mev (the binding energy of the deuteron) between the energy of the elastically scattered pions and that of the most energetic inelastically scattered pions at any angle. With the energy resolution of this experiment this small gap is not observed. At 61 Mev the energy distributions of scattered pions at 45° and 60° do exhibit a peaking at

TABLE III. Lab cross sections (in mb/sterad) for pion scattering with final energy greater than 16 Mev.

Incident energy \ Lab angle	45°	60°	90°	113°	135°	150°
37.6 Mev	0.39±0.15	0.545±0.095	0.635±0.082	0.852±0.087	0.90±0.10	1.12±0.15
60.7 Mev	1.30±0.15	1.051±0.088	1.398±0.083	1.83 ±0.12	2.24±0.12	2.28±0.12

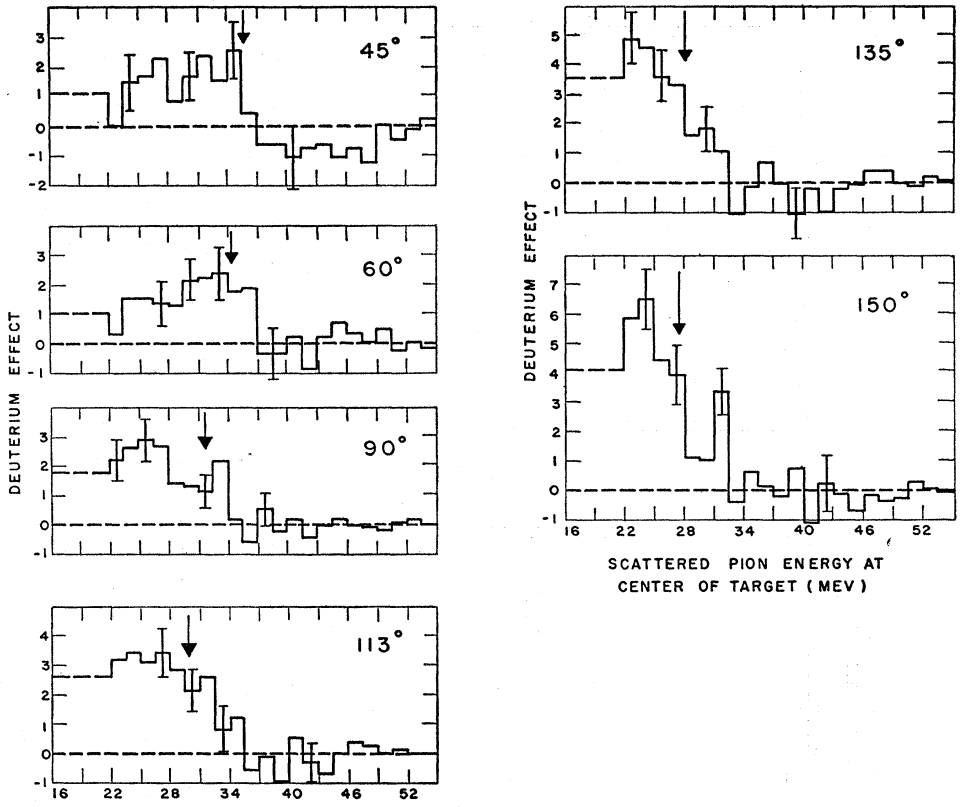

FIG. 8. Energy distribution of scattered pions for incident energy of 37.6 Mev. Arrows indicate the kinematic energy for elastic scattering.

the kinetic energy for elastic scattering (see Fig. 9), but at the other angles the peak is obscured by the large amount of inelastic scattering. Nevertheless, an attempt has been made to separate the elastic scattering at all angles, using the calculated over-all experimental energy resolution. At 38 Mev no attempt was made to extract an elastic cross section because of the poor energy resolution and statistical accuracy of the data.

The following factors enter significantly into the energy resolution:

1. The spread in energy of the incident beam, (± 4 Mev at 38 Mev and ± 3 Mev at 61 Mev).

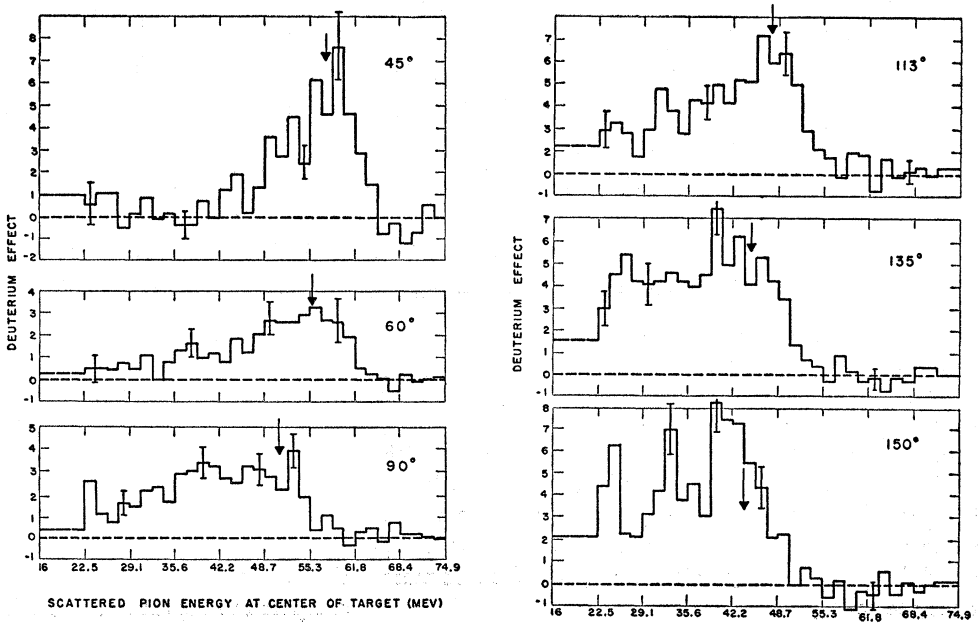

FIG. 9. Energy distribution of scattered pions for incident energy of 60.7 Mev. Arrows indicate the kinematic energy for elastic scattering.

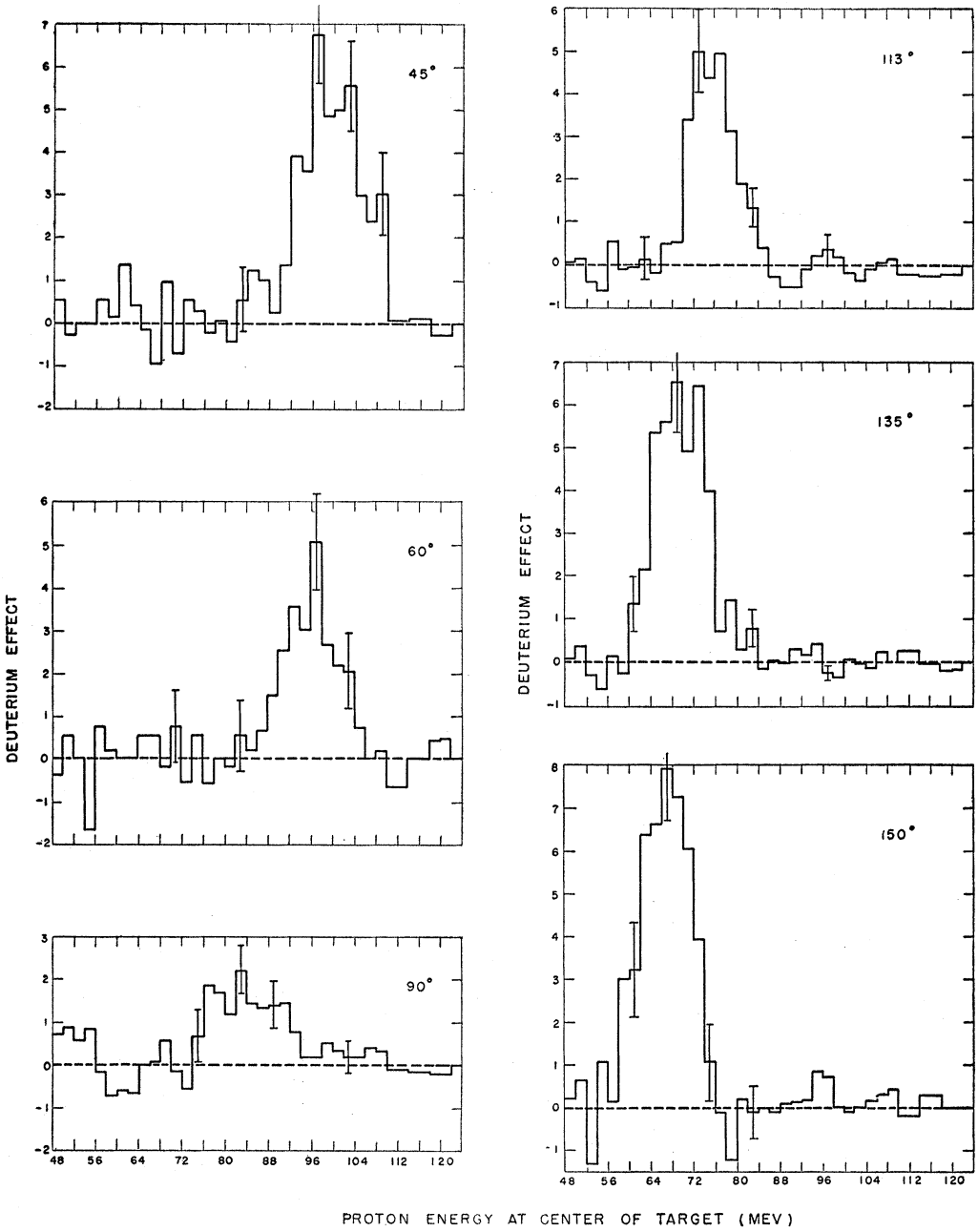

FIG. 10. Energy distribution of emerging protons for incident energy of 37.6 Mev.

2. The variation of energy loss by ionization in the deuterium before and after scattering. For 38-Mev incident pions, the spread varies from ±1 Mev at 45° to ±5 Mev at 150°. At 61 Mev, the variation is from ±0.75 Mev to ±3.5 Mev. The spread increases with angle since, in the forward direction, the sum of losses before and after scattering are approximately constant, while in the backward direction, most of those pions which lose more energy before scattering also lose more after scattering.

3. The energy resolution inherent in the detection system. This is determined to be approximately ±5% from the spreads in the photographically recorded pulse heights produced in counter 5 by the incident beams of 42±4 Mev and 63±3 Mev.

The angular resolution of the detection system, $\pi-\mu$ decay after scattering, and multiple scattering in the deuterium and in counter 3 also effect the energy resolution, but the contributions of these effects is negligible compared to the three major effects mentioned above.

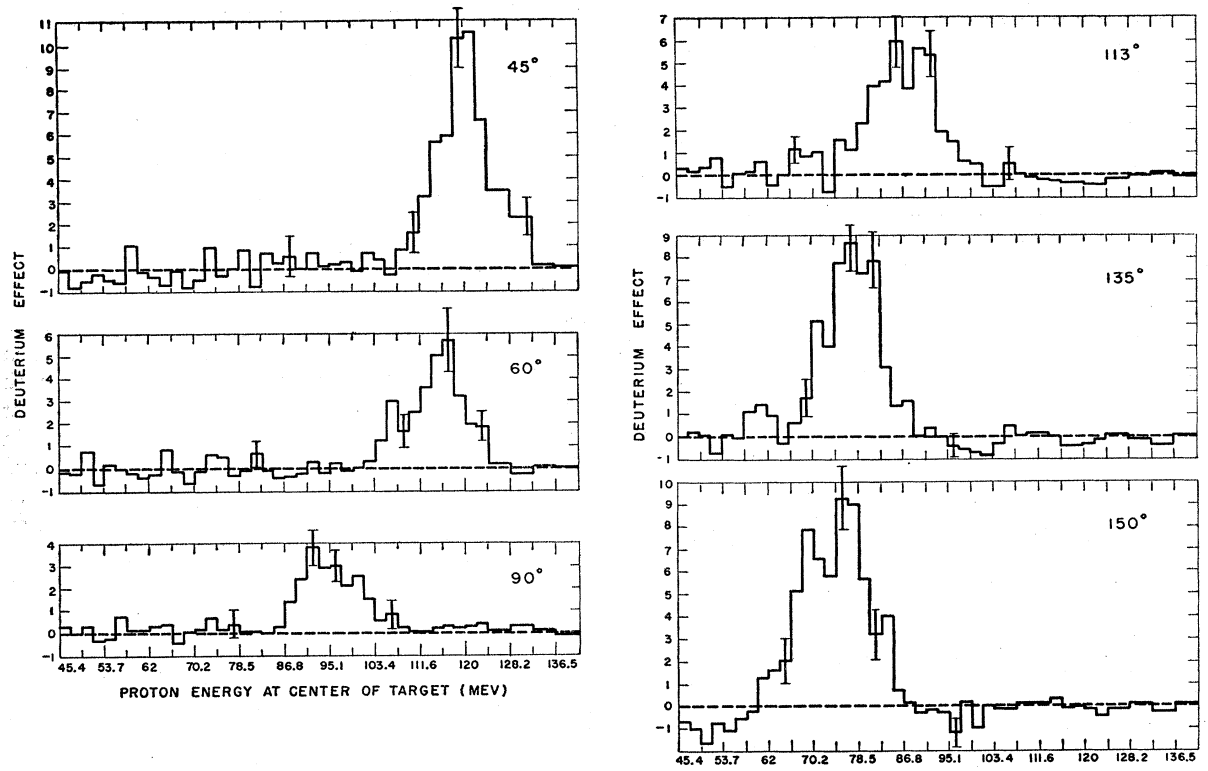

FIG. 11. Energy distribution of emerging protons for incident energy of 60.7 Mev.

The three major contributions to the energy resolution were combined analytically to give an over-all energy resolution function at each of the six scattering angles. The validity of the method used to obtain the resolution functions was tested by filling the target cup with liquid hydrogen and obtaining energy distributions of scattered pions at 60°, 90°, and 135° to the incident 63-Mev π^+ beam. Except for the difference in kinematic energy after scattering, the effects that determine the energy resolution in $\pi-p$ scattering are identical to those in elastic $\pi-d$ scattering. The 90° and 135° energy distributions of pions scattered from hydrogen are presented in Fig. 12. The median energy of each elastic scattering peak agrees to better than ± 1 Mev with the kinematic energy for the process, yielding a check of the energy calibration curves presented in Fig. 6. The calculated resolution functions, normalized to the area under the peaks, are also seen to agree well with the observed shapes. The agreement is also good for the 60° case, which is not shown here.[18] Calculated resolution functions also compared well with the peaks observed on the proton energy distributions presented in Figs. 10 and 11.

In the extraction of an elastic scattering cross section from the deuterium data at 61 Mev, a preliminary elastic cross section is first obtained by doubling the net deuterium effect on the high side of the kinematic energy for elastic scattering, without correcting for the

TABLE IV. Cross sections (in mb/sterad) for nonradiative absorption ($\pi^+ + d \rightarrow p + p$).

Incident energy \ Lab angle		45°	60°	90°	113°	135°	150°
37.6 Mev	$(d\sigma/d\Omega)_{\text{Lab}}$	0.564±0.048	0.331±0.043	0.182±0.027	0.335±0.029	0.523±0.040	0.601±0.049
	$\theta_{\text{c.m.}}$	50.5°	67.0°	98° or 82°	120° or 60°	140° or 40°	153° or 27°
	$(d\sigma/d\Omega)_{\text{c.m.}}$	0.470±0.040	0.038±0.038	0.184±0.027	0.379±0.032	0.648±0.050	0.775±0.063
60.7 Mev	$(d\sigma/d\Omega)_{\text{Lab}}$	0.738±0.046	0.400±0.037	0.286±0.029	0.502±0.046	0.648±0.046	0.811±0.056
	$\theta_{\text{c.m.}}$	51.7°	68.2°	99.5° or 80.5°	121.6° or 58.4°	142° or 38°	154.5° or 25.5
	$(d\sigma/d\Omega)_{\text{c.m.}}$	0.596±0.037	0.344±0.032	0.292±0.029	0.581±0.049	0.834±0.059	1.103±0.076

[18] Differential cross sections obtained for the $\pi^+ + p$ scattering are 0.63±0.13, 1.26±0.08, and 2.83±0.33 mb/sterad at 70°, 101°, and 143°, respectively, in the center-of-mass system. These values agree well with the results of reference 15, corroborating the correction for the attenuation of the background in that experiment, where pulse-height analysis was not used.

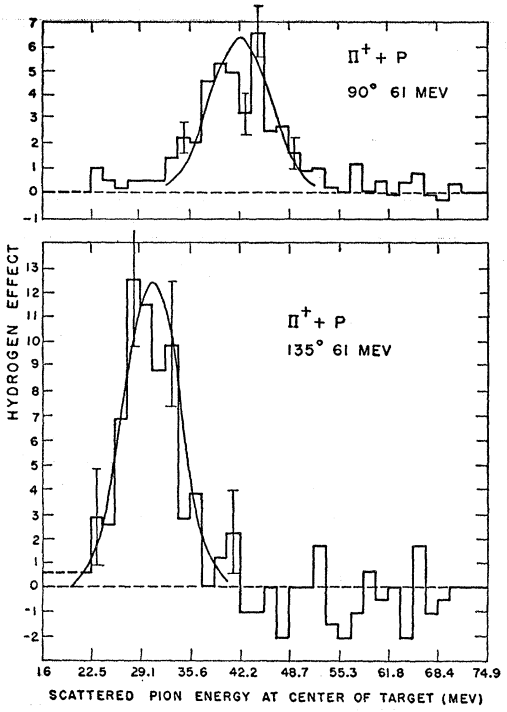

FIG 12. Calculated resolution functions compared to $\pi-p$ scattering results.

possible overlap of high-energy inelastic scattering. Using the resolution function, normalized to this preliminary elastic cross section, the elastic scattering is subtracted out, leaving a preliminary energy distribution for inelastic scattering. By using the resolution function again, an estimate is made of the amount of this inelastic scattering which overlaps into the high side of the elastic peak, and after correcting for the overlap, the final value of the elastic scattering cross section is obtained.

The corrected elastic scattering results are presented in Table V. The errors quoted are obtained by a combination in quadrature of the statistical errors, the errors based on the uncertainty of the inelastic scattering correction, and the errors that would be introduced if the energy calibration, used to obtain the position of the elastic peaks, were in error by ± 1 Mev. The 45° result includes an additional correction, which raised the cross section by 5%, to account for the degradation in energy of a considerable fraction of the background due to the presence of the deuterium. This degradation is most severe at 45° because a large fraction of the high background at this angle is due to essentially full energy scattering from the heavy nuclei in the target and counter 2, and a considerable fraction of this background passes through the deuterium.

VI. DISCUSSION OF RESULTS

A. Nonradiative Absorption Process ($\pi^+ + d \rightarrow p + p$)

Since the final state for this reaction contains two identical particles, the differential cross section in the center-of-mass system must be symmetric about 90°. Therefore all of the data may be presented by plotting the angular distribution between 0° and 90° in the center-of-mass system. (See Fig. 13.) The results are seen to lie on curves of the form $a+b\cos^2\theta$, indicating that only S- and P-wave pions contribute significantly to this reaction at these energies. The fact that points on these plots, which are interspersed between forward and backward laboratory angles, fit on smooth curves, constitutes an additional check on some of the systematics of the measurements. Values of the quantities a and b are obtained by a least squares treatment of the data. The results in millibarns per steradian are $d\sigma/d\Omega = (0.172\pm0.023)+(0.775\pm0.069)\cos^2\theta$ and $d\sigma/d\Omega = (0.244\pm0.024)+(0.985\pm0.079)\cos^2\theta$ at 38 and 61 Mev, respectively. These distributions, integrated from 0° to 180° give total cross sections of 5.41 ± 0.40 and 7.18 ± 0.44 millibarns, respectively. The angular distributions presented here are for cross sections for the process $\pi^+ + d \rightarrow p + p$, and correspond to $\frac{1}{2}$ of the measured cross section for emission of a proton at a certain angle.

By means of the principle of detailed balancing for spin-zero pions the above quoted results for the nonradiative absorption process may be used to obtain cross sections for the inverse process ($p+p\rightarrow\pi^+ + d$). The cross sections obtained in this manner for the pion production process at proton laboratory energies of 355 Mev and 409 Mev are $(0.0153\pm0.0020)+(0.0687\pm0.0061)\cos^2\theta$ and $(0.0270\pm0.0027)+(0.1090\pm0.0089)\times\cos^2\theta$ mb/sterad, respectively. These integrate to give total cross sections of (0.480 ± 0.035) mb and (0.795 ± 0.049) mb, respectively.

References to work on both the production and absorption process prior to mid-1954 are contained in Gell-Mann and Watson and Rosenfeld. More recent work has been done by Cohen,[5] Stadler,[7] Rogers and Lederman,[9] Meshcheryakov *et al.*,[19] and Crawford and Stevenson.[20] The results of this experiment for the total cross sections

TABLE V. Elastic scattering cross sections (61 Mev).

Lab angle	45°	60°	90°	113°	135°	150°
$d\sigma/d\Omega$ (mb/sterad)	0.84 ± 0.20	0.61 ± 0.19	0.50 ± 0.17	1.03 ± 0.23	0.88 ± 0.28	0.95 ± 0.31

[19] M. G. Meshcheryakov *et al.*, Doklady Akad. Nauk. U. S. S. R. **100**, 677 (1955).
[20] F. Crawford and M. Stevenson, Phys. Rev. **97**, 1305 (1955).

and angular distributions at pion lab energies of 37.6 Mev and 60.7 Mev fall on smooth curves drawn through all other experimental points.

Gell-Mann and Watson and Rosenfeld have obtained a semiempirical expression for the variation of the production cross section with energy near threshold.

$$4\pi\frac{d\sigma}{d\Omega}=\alpha\eta+\beta\eta^3\left(\frac{X+\cos^2\theta}{X+\frac{1}{3}}\right), \tag{7}$$

where η=pion momentum in the center-of-mass system in units of μc, and α, β, and X are parameters assumed independent of η. More recently Lichtenberg,[21] has suggested that a more appropriate formula would be

$$4\pi\frac{d\sigma}{d\Omega}=\left(\frac{p_0}{p}\right)^3\left[\alpha'\eta+\beta'\eta^3\left(\frac{X'+\cos^2\theta}{X'+\frac{1}{3}}\right)\right], \tag{8}$$

where p is the relative proton momentum, p_0 is the value of p at threshold, and α', β', and X' are again parameters assumed independent of η. Equations (7) and (8) integrate to give total cross sections:

$$\sigma=\alpha\eta+\beta\eta^3, \tag{7'}$$

$$\sigma=(p_0/p)^3[\alpha'\eta+\beta'\eta^3]. \tag{8'}$$

Crawford and Stevenson[20,22] have made a least-squares fit to both Eqs. (7) and (8), using their experimental differential cross-section measurements near threshold (i.e., $0.3<\eta<0.6$). They obtained

$\alpha=(0.138\pm0.015)$ mb, $\alpha'=(0.125\pm0.017)$ mb,
$\beta=(1.01\pm0.08)$ mb, $\beta'=(1.40\pm0.10)$ mb,
$X=0.082\pm0.034$, $X'=0.13\pm0.03$.

Figure 14 is a plot of Eqs. (7') and (8') using the above values for the parameters. Most of the experimental results, including the results of the present experiment, have also been plotted on the figure. The curves are similar in the region below $\eta=0.6$ because the least-squares fit was made to data only in this region. Above $\eta=0.6$ the curves deviate from one another and neither agrees with the experimental points. This disagreement with experimental values at high values of η is not surprising since α, β, X and α', β', X' are not expected to remain constant far above threshold.[12,21] Lichtenberg concludes from a theoretical calculation that β' should at first slightly decrease and then increase with energy, which would improve the agreement of Eq. (8') with experiment. A fit of Eq. (8') to all of the data below $\eta=1.2$ yields $\alpha'=0.05$, $\beta'=1.68$ (see the solid curve on the figure), although such a fit is quite insensitive to the value of α'. Although this curve is a reasonable excitation function for all the data below $\eta=1.2$, the low value of α' is in apparent contradiction with the value obtained by an indirect method by Brueckner, Serber, and Watson.[23] The resonance or plateau indicated by the data at $\eta\approx1.7$ is not predicted by either of the formulas (7') or (8').

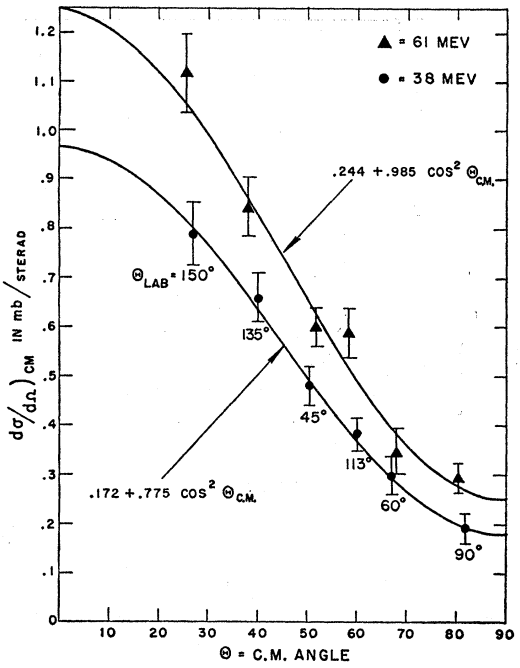

FIG. 13. Center-of-mass cross sections for nonradiative absorption, $(\pi^++d\rightarrow p+p)$. Symmetry about 90° in the center-of-mass system is assumed so that points actually obtained in the backward hemisphere are here shown in the forward hemisphere.

Disagreement between experimental results and the angular distributions predicted by Eqs. (7) and (8) is encountered at even lower η. Equations (7) and (8) may be rewritten in the form

$$\frac{d\sigma}{d\Omega}\alpha A+\cos^2\theta,$$

where

$$A=X+(X+\tfrac{1}{3})(\alpha/\beta)\eta^{-2} \quad \text{for Eq. (7)},$$

$$A=X'+(X'+\tfrac{1}{3})(\alpha'/\beta')\eta^{-2} \quad \text{for Eq. (8)}.$$

Both these equations predict that A should decrease monatonically with increasing η, whereas experimentally A appears to have a minimum at $\eta\approx0.8$.[24] The results of this experiment for A at $\eta=0.721$ and $\eta=0.931$ are (0.223 ± 0.035) and (0.248 ± 0.032), respectively, con-

TABLE VI. Phase shifts used in calculations (degrees).

Incident energy	α_1	α_3	α_{11}	α_{31}	α_{13}	α_{33}
37 Mev	6.89	−3.81	−0.285	−3.81	0.106	3.79
60.7 Mev	9.33	−5.36	0.098	−1.76	−1.96	8.13

[21] D. B. Lichtenberg, Phys. Rev. **105**, 1084 (1957).
[22] F. Crawford and M. Stevenson, Phys. Rev. **107**, 331 (1957).
[23] Brueckner, Serber, and Watson, Phys. Rev. **81**, 575 (1951).
[24] See reference 13, Fig. 2, and also reference 5, Fig. 2.

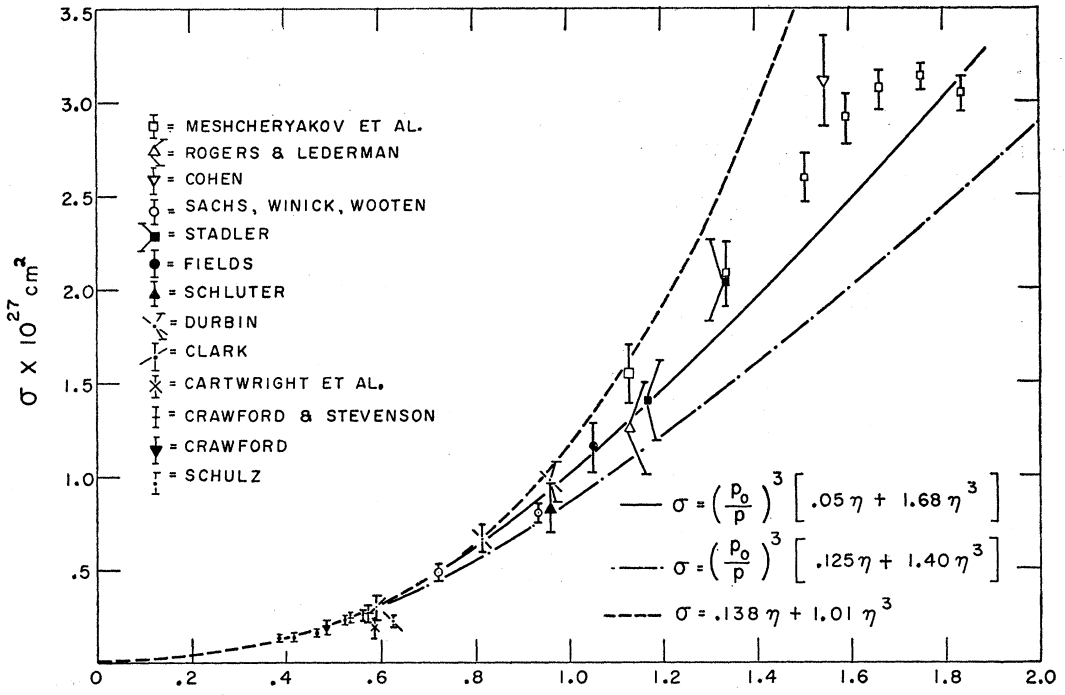

FIG. 14. Summary of the experimental data on total cross section for the process $p+p\rightarrow\pi^+ +d$ at various energies, including results from the inverse process. Data are taken, in the order listed, from references 19; 9; 5; this paper; reference 7; Fields, Fox, Kane, Stallwood, and Sutton, Phys. Rev. **95**, 638 (1954); R. A. Schluter, Phys. Rev. **96**, 734 (1954); reference 4; Clark, Roberts, and Wilson, Phys. Rev. **83**, 649 (1951); Cartwright, Richman, Whitehead, and Wilcox, Phys. Rev. **91**, 677 (1953); reference 20; A. H. Schulz, University of California Radiation Laboratory Report UCRL-1756 (1952).

firming this trend toward increasing isotropy above $\eta=0.8$.

B. Scattering ($\pi^+ +d\rightarrow\pi^+ +d$ and $\pi^+ +d\rightarrow\pi^+ +n+p$)

The impulse approximation,[25–27] originally applied by Chew to *nd* scattering, has been developed and applied to πd scattering by several authors.[10,11,28–34] Most recently Rockmore[11] has used the pure scattering model of Fernbach, Green, and Watson[10] to obtain convenient expressions for the elastic, and the elastic plus inelastic, scattering cross sections including Coulomb effects. These expressions contain no corrections for multiple scattering, absorption, or binding. We have used this formulation to compute impulse approximation predictions for the scattering. The pion-nucleon interactions are inserted via phase shifts and the results obtained are quite sensitive to the choice of these phase shifts. At the lower energy, no experimentally determined complete set of phase shifts is available, so that an interpolated set[35] was used to evaluate Rockmore's equations. At 61 Mev the phase shifts used were essentially those obtained in a machine calculation by Fermi, Metropolis, and Alei,[36] based on the experimental results of Bodansky, Sachs, and Steinberger.[15] Table VI presents the phase shifts used at the two energies. The lower energy calculation was made at 37 Mev.

The results of the calculations for the sum of elastic plus inelastic scattering are presented in Fig. 15. Also indicated for comparison are the sum of the scattering cross sections for positive pions on free protons and neutrons calculated from the phase shifts in Table VI. The points indicated on Fig. 15 are the experimental results from Table III for scattering with emergent pion energy greater than 16 Mev, and hence are not strictly comparable with the theoretical curves. However, at 61 Mev, the pion energy distributions (see Fig. 9) indicate no large inelastic scattering at energies just above our detection threshold. Also, theoretical energy distributions of inelastic scattering[10] of 70-Mev pions at 50° and 100° indicate that the contribution from the energy

[25] G. Chew, Phys. Rev. **80**, 196 (1950).
[26] G. Chew and G. Wick, Phys. Rev. **85**, 636 (1952).
[27] G. Chew and M. Goldberger, Phys. Rev. **87**, 778 (1952).
[28] Fernbach, Green, and Watson, Phys. Rev. **82**, 980 (1951).
[29] J. Blair, Phys. Rev. **83**, 1246 (1951).
[30] B. Segall, Phys. Rev. **83**, 1247 (1951).
[31] K. Brueckner, Phys. Rev. **89**, 834 (1953).
[32] T. Green, Phys. Rev. **90**, 161 (1953).
[33] K. Brueckner, Phys. Rev. **90**, 715 (1953).
[34] S. Drell and L. Verlet, Phys. Rev. **99**, 849 (1955).
[35] H. Anderson, *Proceedings of the Sixth Annual Rochester Conference on High-Energy Physics* (Interscience Publishers, Inc., New York, 1956), PI-20.
[36] Fermi, Metropolis, and Alei, Phys. Rev. **95**, 1581 (1954).

range below 25 Mev is negligible. Therefore, at 61 Mev, it is likely that no substantial addition, to account for inelastic scattering below 16 Mev, needs to be made to the experimental points in comparing them with the theory. At 38 Mev, the energy interval below the 16-Mev threshold constitutes a larger fraction of the energy range available for inelastic scattering. The energy distributions at 38 Mev indicate that the inelastic scattering has not fallen appreciably at 16 Mev. (See Fig. 8.) Therefore it is difficult to estimate the addition that should be made to the experimental points at 38 Mev to account for inelastic scattering below 16 Mev.

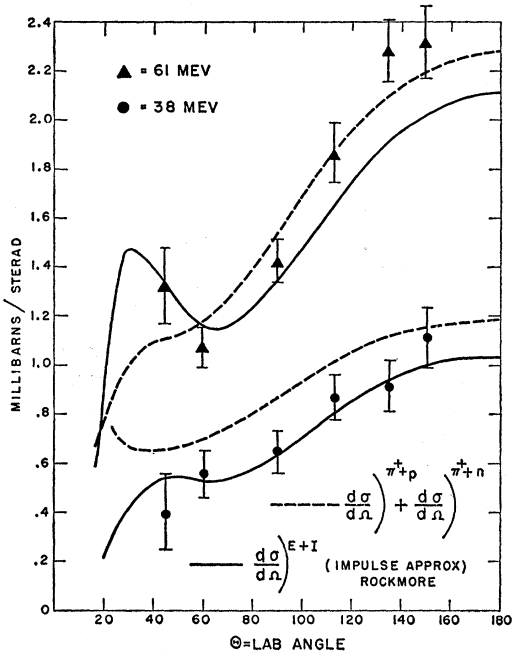

FIG. 15. Impulse approximation curves for elastic plus inelastic scattering and experimental results for scattering with final pion energy greater than 16 Mev. For comparison, the sum of $\pi^+ + p$ and $\pi^+ + n$ cross sections are also shown.

The results of an impulse approximation calculation for the elastic scattering at 61 Mev are presented in Fig. 16, along with the experimental cross sections listed in Table V.

At 61 Mev, both the elastic and elastic plus inelastic impulse approximation curves are lower than the experimental points in the backward direction. In order to explain this discrepancy on the basis of errors in the phase shifts used in the 61-Mev impulse approximation calculations, it is necessary to change the phase shifts by amounts inconsistent with the statistical accuracy of the experimental $\pi - p$ data from which these phase shifts were obtained. Rockmore[11] has estimated corrections to the impulse approximation for the effects of multiple scattering, absorption, and binding at 85 Mev. Although the corrections obtained for multiple scattering and binding are of the order of 10% at 85 Mev, they are of opposite sign so that the net correction is small.

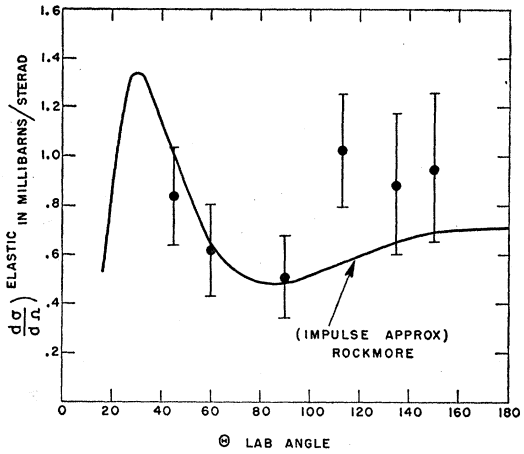

FIG. 16. Impulse approximation curve and experimental results for elastic scattering at 61 Mev. The large errors are mainly the result of an estimate of the systematic errors involved in the process of extracting the elastic cross sections.

ACKNOWLEDGMENTS

We would like to express our appreciation to Miss C. Macleod for assistance in analyzing data and performing calculations, Mr. E. L. Koller and Mr. S. Penman for assistance during experimental runs, Dr. R. Rockmore for helpful discussions concerning the impulse approximation and assistance in some of the calculations, Professor E. T. Booth and Mr. D. Koppel for use of the magnetic channel, Dr. A. Hutchison of Argonne National Laboratory for an analysis of the deuterium, and the entire staff of the Nevis Cyclotron Laboratory for cooperation and aid during the course of the experiment, especially Mr. R. Parker for preparing the liquid hydrogen.

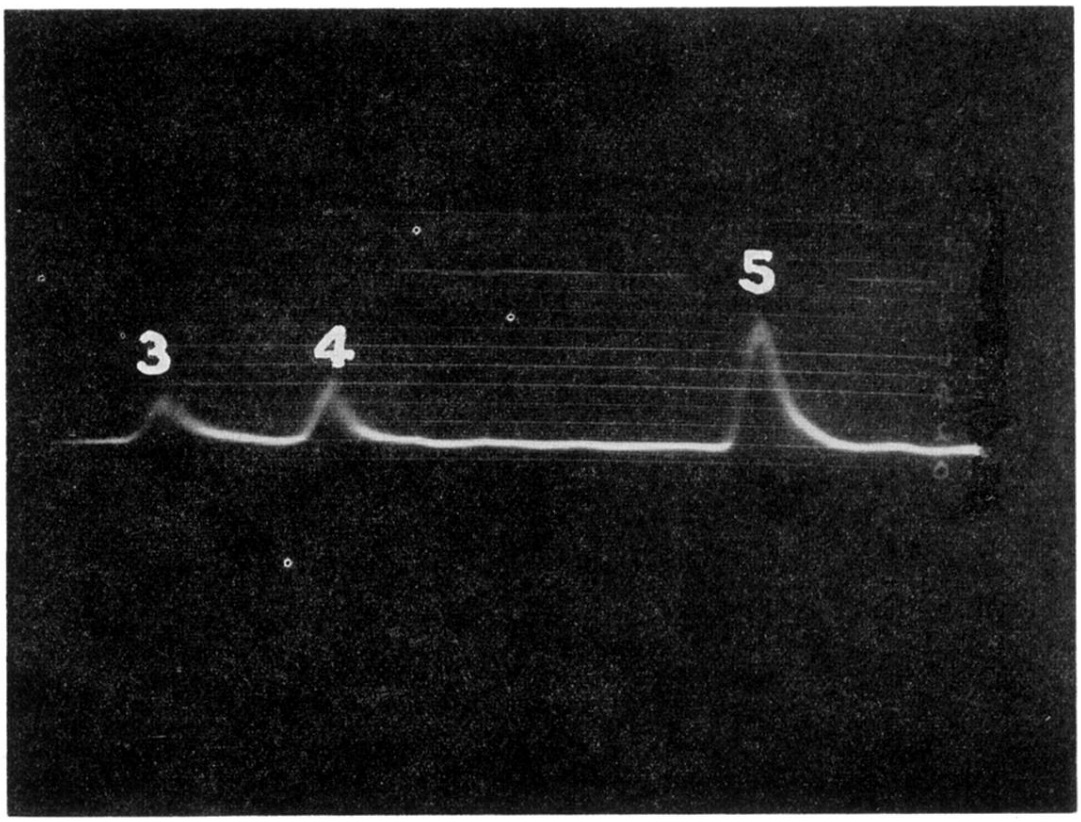

FIG. 7. Typical polaroid photograph of oscilloscope traces at 0 deg.